Title: **Differential effect of low and high frequency transcranial magnetic stimulation on cortical excitability and myelination after neonatal hypoxia in mice.**

Rafael Bandeira Fabres[1], Ivan Goussakov[1], Sylvia Synowiec[1], Vasiliy Yarnykh[2], Daniil Aksenov[3], Alexander Drobyshevsky[1]*

Author names and affiliations:
[1]Department of Pediatrics, Endeavor Health, Evanston, IL, 60201, USA

[2]Department of Radiology, University of Washington, Seattle, WA, 98195, USA

[1]Department of Radiology, Endeavor Health, Evanston, IL, 60201, USA

Corresponding author email: adrobyshevsky@northshore.org
Conflict of interest statement: "The authors declare no competing financial interests."
Acknowledgments: This study was funded by NIH grants 1R01NS119251-01A1

Keywords: myelination, perinatal brain injury, transcranial magnetic stimulation

ABSTRACT

Premature infants are highly susceptible to intermittent hypoxic brain injury, which is associated with adverse motor, cognitive, and behavioral outcomes, including deficits in attention, hyperactivity, and learning. Previous animal studies have shown myelination deficits and increased glutamatergic synaptic strength in the sensory-motor cortex. The study investigates the feasibility, safety, and therapeutic potential of repetitive transcranial magnetic stimulation (rTMS) in ameliorating central hypomyelination, reducing excessive glutamatergic transmission in cortical neurons following neonatal intermittent hypoxia (IH), and improving behavioral outcomes.

In the mouse model of neonatal intermittent hypoxia, low-frequency (LF-rTMS) stimulation at 1 Hz or high-frequency (HF-rTMS) at 10 Hz stimulation was applied for 5 days shortly after the IH injury. The rTMS regimen did not induce apoptosis or inflammation. HF-rTMS significantly ameliorated hypomyelination in the corticospinal tract, with a larger increase in MPF in the stimulated hemisphere and also in the contralateral hemisphere. LF-rTMS reduced locomotor hyperactivity in female IH mice and decreased elevated glutamatergic synaptic excitability in motor cortex slices. This study provides evidence that rTMS can modulate both myelination and synaptic excitability, leading to improved behavioral outcomes after neonatal hypoxic brain injury. These findings highlight the therapeutic potential of rTMS as an early intervention strategy for neurological sequelae of perinatal hypoxia.

INTRODUCTION

Premature infants are highly susceptible to hypoxic brain injury, which is associated with adverse neurological outcomes. A primary cause of motor deficits following perinatal hypoxic brain injury, including cerebral palsy, is disrupted ascending and descending functional motor control due to white matter injury (WMI) affecting axons and myelin sheaths (Volpe 2008, Babcock, Kostova et al. 2009), particularly in the posterior limb of the internal capsule (IC), where corticospinal tract (CST) fibers descend (Hunt, Neil et al. 2004). Although efforts continue to mitigate cellular damage following brain injury, treatment options for established motor deficits remain primarily palliative, with many therapies for spasticity and motor control abnormalities focusing on symptom management rather than addressing underlying causes (Milner-Brown and Penn 1979, Downing, Ganley et al. 2009, Poon and Hui-Chan 2009). Early

restoration of myelination and normal functional connectivity within motor control pathways is therefore crucial for preventing the formation of pathological circuits in infants with perinatal brain (Cahill-Rowley and Rose 2014, Sukal-Moulton, Krosschell et al. 2014).

Early interventions that stimulate motor control can be enhanced with neuromodulatory interventions, such as non-invasive brain stimulation (NIBS), specifically repetitive transcranial magnetic stimulation (rTMS), to promote functional connectivity in motor control pathways. NIBS has demonstrated a high margin of safety in pediatric settings (Gillick, Feyma et al. 2013, Gillick, Gordon et al. 2018). While showing promise in treating pediatric neurological conditions like stroke, epilepsy, and unilateral cerebral palsy (Krishnan, Santos et al. 2015), its potential for promoting myelination early after perinatal brain injury requires further exploration. The current study investigates the feasibility and effectiveness of rTMS in promoting activity-dependent CST myelination.

In addition to motor abnormalities, adverse cognitive outcomes, including deficits in memory, attention, and executive function, are common after perinatal hypoxic brain injury (Ketzer, Gallois et al. 2012, Burnett, Scratch et al. 2013, Anderson 2014, Johnson and Marlow 2017, Mikkelsen, Olsen et al. 2017). Animal studies (Goussakov, Synowiec et al. 2019) indicate that hyperactivity and learning deficits following neonatal intermittent hypoxia (IH) are linked to an abnormal increase in glutamatergic synaptic strength (synaptic potentiation), resulting in the occlusion of synaptic plasticity, a process crucial for brain development and cortical network formation. This highlights the need for therapeutic interventions that can target and potentially restore normal synaptic function.

While pharmacological approaches to excessive glutamatergic transmission face limitations due to potential disruptive consequences of long-term global inhibition on the developing brain, non-invasive neuromodulation offers a valuable alternative. However, the long-term effects and optimal stimulation parameters of NIBS on the developing brain remain unknown. This study examines the differential effects of low- and high-frequency repetitive transcranial magnetic stimulation (rTMS) on cortical excitability and myelination in mice following neonatal hypoxia. We hypothesize that low-frequency rTMS can reduce excessive glutamatergic transmission in cortical neurons following neonatal intermittent hypoxia (IH), thereby restoring synaptic plasticity, excitatory-inhibitory balance, and improving behavioral outcomes. Furthermore, we aim to investigate the feasibility and effectiveness of rTMS in promoting central CST myelination.

METHODS

The study has received approval from the Institutional Animal Care and Use Committees of Endeavor Health. The timeline of the experiments is shown in Figure 1.

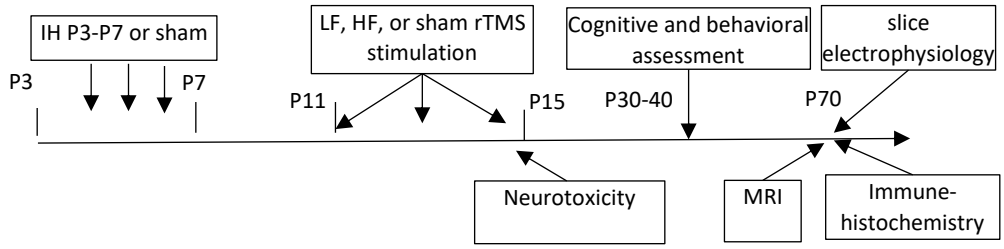

Figure 1. Timeline of the experiments.

Neonatal intermittent hypoxia

C57BL/6J mice were obtained from the Jackson Laboratory (Bar Harbor, Maine) and bred at the Endeavor Health animal facility. Neonatal mice of both genders were randomly assigned to the IH or Normoxia groups. Animals underwent an intermittent hypoxia regimen using cycles of hypoxia with a 5% O_2 / 95% N_2 gas mixture for 2.5 minutes, followed by 5 minutes of normoxia with room air (Goussakov, Synowiec et al. 2019). During hypoxic exposure, pups were separated from their dams and placed into a 250 mL air-tight chamber in a temperature-controlled neonatal incubator with an ambient temperature of 35 °C. The paradigm began at postnatal day 3 (P3) and continued for five consecutive days. Airflow was maintained at 4 L/min and switched between the hypoxic mixture and room air using solenoid valves controlled by a programmable timer. Oxygen concentration and air temperature within the chamber were continuously monitored with calibrated sensors, reaching a nadir of 5% O_2 within 40 seconds during hypoxic periods. The total number of daily hypoxic episodes gradually decreased across the 5 days (20, 18, 11, 9, and 8), divided into morning and afternoon sessions. Between sessions, pups were returned to their dams for 4 hours to recover and nurse. Normoxia mice underwent similar handling procedures, but remained in room air inside the incubator throughout the experiment. Mortality after neonatal IH was 28.5 %. The number of animals is indicated below for each outcome measure.

Transcranial magnetic stimulation

At P11, mice were randomly assigned to groups undergoing repetitive transcranial magnetic stimulation (rTMS) or sham treatment (n = 8, 7). rTMS was applied to non-sedated mouse pups using the Neurosoft Transcranial Magnetic Stimulator (Soterix Medical Inc., Woodbridge, NJ) and liquid-cooled 58x35 mm figure-of-eight TMS coil, optimized for unilateral stimulation rodent experiments (Boonzaier, Petrov et al. 2020). The coil is capable of delivering 2.6T at 80% power. The stimulation was delivered as a train of pulses over 10 minutes, twice a day, with 4 hours between sessions, for 5 days from P11 to P15. Stimulation groups consisted of Low Frequency (LF-rTMS, 1 Hz pulse train frequency, 600 pulses per session), High Frequency (HF-rTMS, 10 Hz for 6 seconds, 54 seconds of rest, 600 pulses per session), and Sham stimulation (n = 8, 7) with the same animal setup but without stimulation. The mouse's head was immobilized in a custom-printed helmet (Figure 1), and its body was lightly swaddled in gauze to minimize motion. The TMS coil was centered 5 mm above the bregma to target the

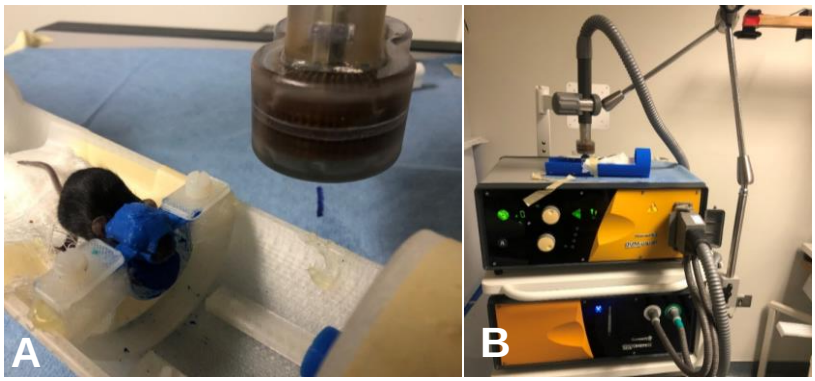

Figure 1. A. Application of transcranial magnetic stimulation on a P12 mouse pup with a dedicated actively cooled rodent 25 mm TMS coil. A custom helmet enables pup head immobilization for rTMS. B. View of the stimulator experimental setup.

sensorimotor cortex bilaterally. Stimulation was set to 70% of the maximum apparatus power, approximately 10% below the motor response evoked with a single pulse. Motor responses were visually observed by hind limb and tail twitching (Supplementary video 1). Mice in sham control groups (n=8,7) were head immobilized for the same duration but not stimulated. To reduce stress, mouse pups were habituated to the procedure the day before stimulation began by being handled and gently restrained for 5 minutes.

In vivo MRI methods.

Ten-week-old mice were sedated with isoflurane (Abbot, IL) inhalation, diluted in air to 5% for induction and 1.5% for maintenance. The animal's respiration rate and rectal temperature were monitored with a small animal physiological monitor (SAII's Small Animal Instruments, NY, USA). Body temperature was maintained at 35 °C by blowing warm air from a temperature control unit. Animals were placed prone in a cradle and imaged in a 9.4 T Bruker Biospec system (Bruker, Billerica, MA). The receiver coil was a 16 mm diameter, linear surface coil (Doty Scientific, Columbia, SC). The transmitter was a 70 mm quadrature volume coil.

Macromolecular proton fraction (MPF) mapping and processing.

3D MPF maps were obtained from three source images (Magnetization transfer (MT)-, Proton density (PD) -, and T1-weighted) using a single-point methodology with synthetic reference images (Yarnykh 2016). PD- and T1-weighted GRE images were acquired with TR/TE = 16/3 ms and α = 3° and 16°, respectively. MT-weighted images were acquired with TR/TE = 22.5/3 ms and α = 8°. The off-resonance saturation pulse was applied at the offset frequency of 4.5 kHz with an effective saturation flip angle of 500°. All images were acquired in the axial plane with whole-brain coverage and a resolution of 0.15x0.15x0.3 mm^3. All images were obtained with four signal averages. All 3D imaging experiments employed a linear phase-encoding order with 100 dummy scans, slab-selective excitation, and a fractional (75%) k-space acquisition in the slab selection direction. To correct for field heterogeneities, 3D B0 and B1 maps were acquired using the dual-TE (TR/TE1/TE2 = 20/2.9/5.8 ms, α = 8°) and actual flip-angle imaging (AFI) (TR1/TR2/TE = 13/65/4 ms, α = 60°) methods, respectively (Yarnykh 2007). Imaging time was 26 min. All reconstruction procedures were performed using custom-written C-language software available at https://www.macromolecularmri.org/.

Magnetization transfer images of mouse brains, obtained as part of an in vivo MPF experiment and exhibiting excellent white/gray matter contrast, were used for automatic structural parcellation using a multi-atlas label fusion method, as detailed in (Ma, Cardoso et al. 2014). Briefly, individual mouse head images were processed for brain extraction, intensity non-uniformity correction, affine registration to atlas images, and label fusion. The publicly available MRMNeAt atlas database was used, containing 10 individually labeled C57BL/6J in vivo mouse brains. Values of MPF in twenty-one white and gray matter structures from the atlas were extracted for individual animals.

Ex vivo field excitatory postsynaptic potential (fEPSP) recordings in motor cortex.

Electrophysiological studies were in adult mice after completion of behavioral and MRI studies at P70, n=4 mice per experimental group. Mice were deeply anesthetized with isoflurane (3%) and decapitated. Brains were rapidly removed in ice cold artificial spinal fluid (aCSF) of the following composition (mM): 124 NaCl, 2.5 KCl, 25 NaHCO3, 2 CaCl2, 2 MgSO4, 1.25 NaH2PO4, 10 HEPES, 10 D-glucose, bubbled with carbogen (95% O2/5% CO2) to maintain pH of 7.4. Osmolarity of this solution was 300±5 mOsm. Slices containing motor

cortex were cut 300 µm thick using a Leica vibrotome (VT1000S, Leica Biosystems). Slices were maintained in an incubation chamber filled with room temperature 21ºC aCSF and bubbled with carbogen for at least 1 hour before recording. The same aCSF solution was used during recording and perfused 3 mL/min at 21ºC. All drugs were purchased from Sigma-Aldrich Inc. (MO, USA). After incubation for at least one hour, the slices were transferred to a submerged recording chamber model RC-24 (Warner Instruments, Hamden, CT, USA) and perfused at a rate of 3 ml/min by gravity. At this rate, the 500 µl volume of the recording chamber is refilled in 10 seconds. A glass recording electrode, filled with aCSF was placed in the middle of layer six of the M1 cortex. A bipolar stimulation electrode, composed of tightly twisted 25 µm diameter platinum/iridium wires, was placed 200-400 µm away from the recording site in the middle of the molecular layer. The distance between the electrodes was adjusted to avoid pop spikes that may otherwise introduce secondary activation by firing stimulated afferent cells at all ranges of stimulation intensity, 0-700 µA. Input-output curves were constructed by plotting the amplitude as a function of the stimulation intensity. Stimulus pulses with 0.1 ms width were delivered from the stimulus isolator. Stimuli to evoke fEPSP were applied once per minute in all recordings. All recordings were obtained using a patch-clamp amplifier, the Multiclamp 700B (Molecular Devices), with the low-pass filter disabled to measure the direct current potential from the sweep baseline. A pipette potential offset was applied immediately to the solution before slicing the preparation. The high-pass filter of the amplifier was set to 3 kHz to improve the resolution of the initial slope. The Digidata 1442 was used to sample data points at 100 kHz, and the data were analyzed using pClamp 10.1 software (Molecular Devices). Input-output curves were generated by increasing stimulus intensity in 20 µA increments from 0 to 300 µA and recording fEPSP responses. Paired pulse facilitation (PPF) was elicited by applying two consecutive stimuli 70 ms apart. PPF was expressed as a ratio of the amplitudes of the second fEPSP to the first.

Behavioral studies.

All behavioral testing procedures were conducted in a dedicated quiet room during the daytime between 30 and 40 days of age. Each apparatus was thoroughly cleaned with 70% ethanol and allowed to air for 3 minutes between animals. Animal movements were tracked and analyzed using ANY-maze software version 7.3 (Stoelting Co., Wood Dale, IL, USA).

Open Field Test: Mice (n=6 per experimental group for female and male mice) were placed individually in the center of a clear, open-field box (61 x 61 cm) and allowed to explore freely for 20 minutes. The software automatically recorded the following parameters of spontaneous locomotor activity: total mobile time, mean speed, total distance traveled, and time spent in the center zone (40 x 40 cm) compared to the peripheral zone. The center zone time is often used as an indicator of anxiety-like behavior in rodents.

Rotarod Test: Motor coordination and balance were assessed using a 4-day accelerating Rotarod test (Harvard Apparatus, Holliston, MA, USA). Mice were placed on a textured rotating rod (3.2 cm diameter) with individual lanes to prevent interaction. The rotarod began at an initial speed of 4 revolutions per minute (rpm) and gradually accelerated to 40 rpm over 5 minutes. Each mouse underwent four trials per day for four consecutive days, with an inter-trial interval of at least 15 minutes. The latency to fall from the rod (in seconds) was recorded for each trial, with a maximum cutoff of 300 seconds. Performance was evaluated by calculating the average latency to fall across trials for each day, providing a measure of motor learning and coordination over time.

Cell injury assessment on Real-time PCR.

A subset of mice (n=4 per group) was euthanized at P15, the last day of the rTMS course. Brains were collected and individually frozen in liquid nitrogen and stored at -80°C before use. The tissue was homogenized in Qiazol Lysis Reagent (cat. # 79306 Qiagen, Germantown, MD) on ice for the extraction of total RNA. The NanoDrop (ThermoFisher Scientific, USA) instrument was used to measure RNA quantity and quality. 500 ng of isolated total RNA was used to synthesize cDNA using an RT2 First Strand Kit from QIAGEN. cDNA was amplified by polymerase chain reaction (PCR) with QuantiTect Sybr Green PCR Kit (Qiagen, Germantown, MD) on an Applied Biosystems QuantStudio 7 Flex real-time quantitative PCR instrument. The total reaction volume of 25 µL consists of 1.0 µl RT product (cDNA). Primers for Caspase-3, IL-1β, IL-6, TNF-α, and GAPDH for the SYBR Green Assay were predesigned and ordered from Integrated DNA Technologies, Inc., USA. For each primer, the final concentration was 0.4 µM, and the annealing temperature was adjusted accordingly. Gene expression was normalized to the housekeeping gene GAPDH and expressed as a fold change using the ΔΔCt method.

Immunohistochemistry and assessment of OL subpopulations.

Mice were euthanized P70 by transcardial perfusion with saline solution (0.9% NaCl) followed by 4% paraformaldehyde (PFA). Brains were removed and post-fixed in 4% PFA overnight, soaked in 30% sucrose solution for cryoprotection, frozen on dry ice, and cryosectioned 20 µm in the coronal plane.

To identify myelin, oligodendrocyte progenitor cells (OPCs), maturing oligodendrocytes, and astrocytes, primary antibodies against MBP (AB218011), NG2 (ab275024, Abcam), Olig2 (ab9610, Millipore), and GFAP (ab4674, Abcam) were used, respectively. Sections were then incubated with the appropriate fluorescent secondary antibodies conjugated to Alexa Fluor 488 anti-rabbit (ab150077, Abcam) or Alexa Fluor 488 anti-chicken (ab1510169, Abcam) for 1 hour at room temperature. Afterward, the sections were mounted with DAPI-containing mounting medium (VECTASHIELD, H-1200-10). Negative controls were processed by incubating some sections with only the secondary antibodies. All samples were processed simultaneously and incubated for the same duration to ensure consistency.

Images of the corpus callosum, internal capsule, and cerebral cortex (20x magnification) were acquired using a Nikon E600 microscope. For cell counting and fluorescence intensity analysis, a region of interest (ROI) of 3800 µm² was drawn on each slice to delimit the areas of interest. For the analysis of MBP-staining fluorescence intensity, the mean background intensity was calculated for each image using small regions of interest (ROIs) placed in areas devoid of MBP-positive fibers. This background value was then used to correct the fluorescence signal within the defined ROIs, allowing for normalization and comparison across groups. A semi-quantitative analysis of GFAP-, NG2-, and Olig2-positive cells was performed. Samples from three animals per group were analyzed to estimate the number of astrocytes, OPCs, and oligodendrocytes. For each animal, five sections were evaluated using the Cell Counter plugin in ImageJ (available at https://imagej.net/Downloads). All image acquisition and quantification procedures were conducted by an investigator blinded to the experimental groups to ensure unbiased analysis.

Statistical analysis.

A two-way ANOVA was used to test the main effects of rTMS and IH factors, as well as their interactions, on gene expression of apoptotic and proinflammatory cytokines. Analysis was performed using GraphPad Prism, GraphPad Software, version 10.5, La Jolla, CA, USA.

RESULTS

rTMS does not induce apoptosis and inflammation in neonatal mice

Analysis of gene expression for the apoptotic marker Caspase-3 and pro-inflammatory cytokines TNF-α, IL-1β, IL-6, and did not reveal significant effects for the main factors IH, rTMS stimulation, and their interactions (Fig.1). The results confirm previous findings of little cell death in the neonatal chronic IH model (Goussakov, Synowiec et al. 2019) and indicate no apoptotic or pro-inflammatory effects ($F_{2,22}$=0.47, p-val 0.69 for Caspase-3, $F_{2,22}$=0.50, p-val 0.61 for IL-1β, $F_{2,22}$=2.50, p-val 0.10 for IL-6,) of the performed rTMS regimen on neonatal mouse brain.

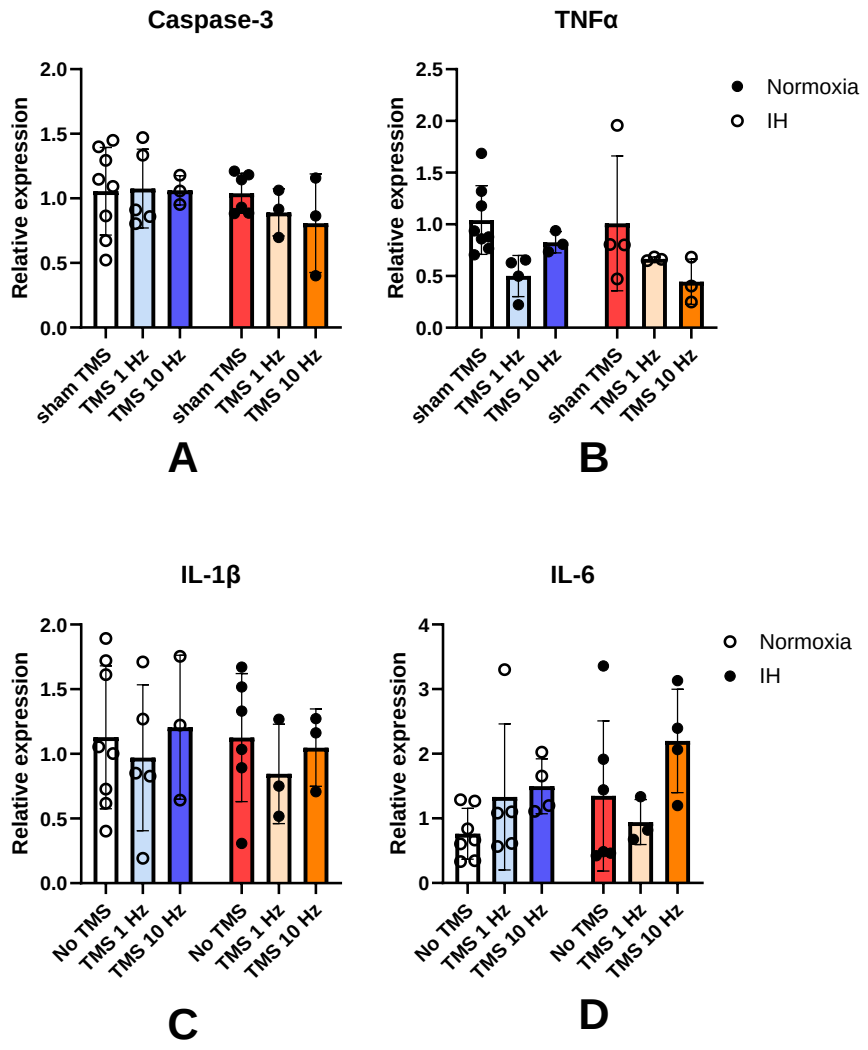

Figure 2. rTMS did not induce apoptosis and inflammation in neonatal Normoxia and IH mice. Relative expression of genes to housekeeping gene GAPDH, determined by RT-PCR, is shown for apoptotic marker caspase-3 (A) and pro-inflammatory markers TNFα (B), IL-1β (C), and IL-6. No significant main effects on IH and rTMS on 2-way ANOVA. Data are shown as mean ± SD.

There was a decrease of TNF-α after rTMS in the IH group (rTMS main effect $F_{2,22}$=4.2, p-val 0.029).

HF-rTMS ameliorates hypomyelination after neonatal IH in the corticospinal tract.

Representative MPF maps for the sham and HF-rTMS mice are shown in Figure 3. Note a bilateral increase in myelin content in the internal capsule of the stimulated mouse (Figure 3B, arrow).

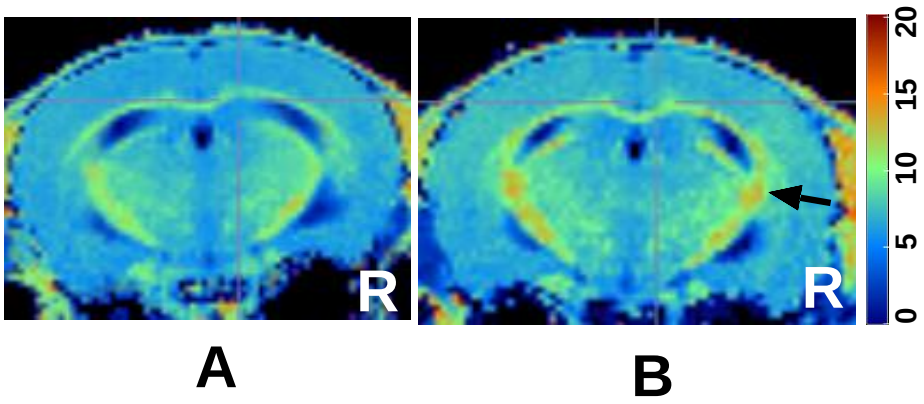

Figure 3. MPF maps in sham (A) and 10 Hz rTMS mouse (B). The arrow points to the internal capsule in the right hemisphere, which was targeted for stimulation. The color bar indicates the macromolecule proton fraction for the pseudo-colored maps in % values.

The main effects of the IH ($F_{(2,38)}$ = 6.42, p=0.0039) and rTMS($F_{(1, 38)}$ = 5.18, p=0.028) factors and their interaction ($F_{(2,38)}$ = 3.31, p=0.043) were significant on 2-way ANOVA in MPF in the right internal capsule in the hemisphere that was targeted for the rTMS stimulation (Figure 3 A). Post-hoc comparison revealed a larger increase in myelination with HF-TMS (p=0.004) and a smaller increase in LF-rTMS (p=0.031) relative to sham stimulation in the IH group. A decrease of myelination after IH and the effect of rTMS stimulation (IH ($F_{(2,38)}$ = 3.30, p=0.047) and rTMS($F_{(1, 38)}$ = 7.10, p=0.012) was also observed in the internal capsule of the other hemisphere (Figure 3 B). Post-hoc multiple comparisons were significant between LF-rTMS groups (p=0.046). No significant effects of IH and TMS stimulation were found in the corpus callosum and cerebral cortex (Figure 3C, D).

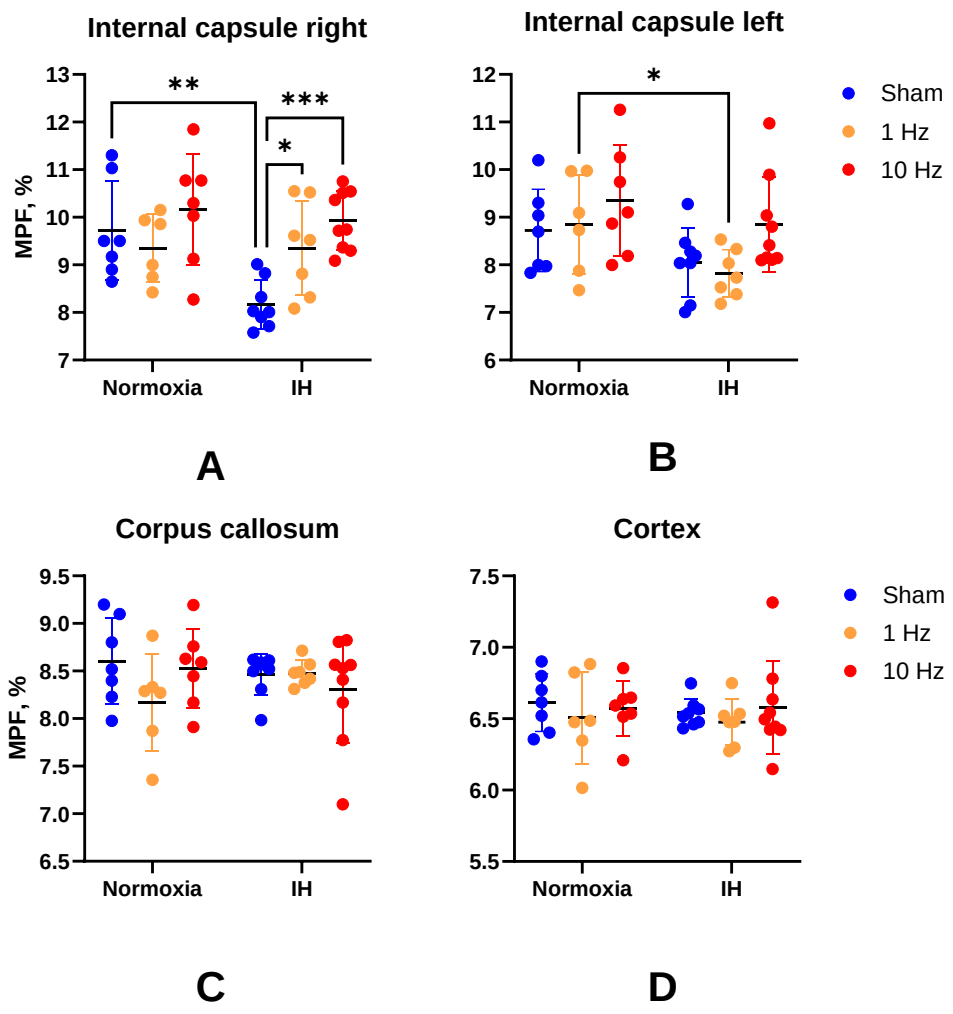

Figure 4. Macromolecule proton fraction group 2-way ANOVA with post-hoc multiple comparisons. A. Internal capsule right (stimulated) and left (B). No significant main effects in IH and rTMS in Corpus callosum (C) and Cortex (D) on 2-way ANOVA. Data are shown as mean ± SD.

Low-frequency rTMS reduces locomotor hyperactivity after neonatal IH.

Female and male mice were analyzed separately in the open field test. After neonatal IH, female mice exhibited hyperactivity, characterized by increased locomotion speed, more time spent mobile, and a greater traveled distance, as shown in Figure 5A (post-hoc comparisons of means p=0.016). However, the overall main effect of IH on traveled distance was not significant in the 2-way ANOVA ($F(1, 30) = 1.61$, $p = 0.21$). The main effect of rTMS was significant ($F(1, 30) = 4.39$, $p = 0.044$), although the interaction between IH and rTMS was not significant ($F(2,30) = 2.80$, $p=0.076$). Additionally, there were no significant effects of IH and stimulation, nor differences between the experimental groups for travel distance in male mice.

Analysis of time spent in the center area of the open field arena, recorded as an index of anxiety, did not reveal overall significant main effects for IH and stimulation, except the

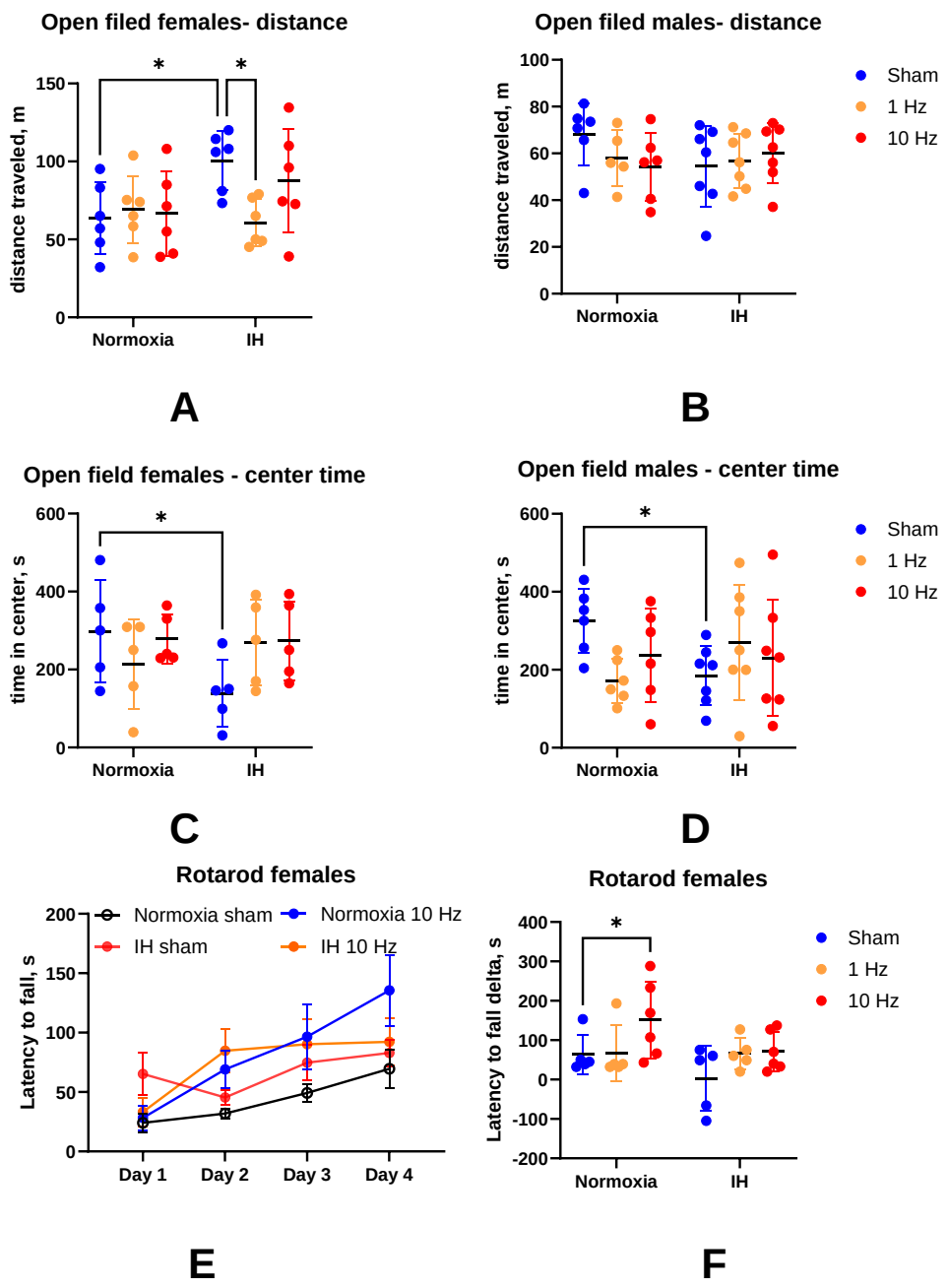

Figure 5. Behavioral tests in mice after neonatal IH and rTMS stimulation on 2-way ANOVA. A,B - Travel distance in open field test for female (A) and male mice(B). C,D – Time spent in the center zone in the open field test for female (C) and male mice (D). Data are shown as mean ± SD. E. Latency to fall on rotarod test from day 1 to day 4 of testing, D. A change of latency to fall from day 1 to day 4. *- $p<0.05$, post hoc test on 2-way ANOVA

interaction term in males ($F_{(2,33)} = 3.61$, $p=0.038$). The mean time spent in the center zone was significantly less for the IH sham groups for females and for males (Figure 5C,D, post-hoc $p<0.05$), but there was no difference with the sham groups after rTMS, indicating anxiolytic effect of rTMS after neonatal IH.

High-frequency rTMS enhances motor learning in Normoxia mice but not after neonatal IH.

Latency to fall increased from day 1 to day 4 in all experimental groups, indicating motor learning in coordination and balance (Figure 5 E, show for females), with significant factors days of test ($F_{(3,99)} = 13.413.61$, $p<0.001$) and treatment-by-day of test interaction ($F_{(9.,99)} = 2.88$, $p=0.048$) on repeated measures ANOVA. There was no difference in the latency to fall on day 1, but the increase in the latency to fall depended on the treatment group (Hypoxia factor $F_{(2,26)} = 3.57$, $p=0.042$ on 2-way ANOVA). It was the most prominent in Normoxia HF-rTMS group in females relative to Normoxia sham (post-hoc $p=0.045$, Figure 5F). There was no significant difference in the motor learning index for males between the experimental groups on the rotarod test.

rTMS reduces increased glutamatergic transmission after neonatal IH.

The sequence of field responses on stimulation in layer 6 of motor cortex perfused slice preparation, consisting of the short latency volley burst (VB) followed by the first short latency fEPSP and often by the longer latency second fEPSP, was reproducible in all subgroups and observed in both control aCSF and after PTX application (Fig.6A). The VB was insensitive to neurotransmitter receptors blockade and was presumed to be presynaptic. The later components, first and second field potentials, were completely blocked by 50 µM CNQX and reflected monosynaptic (latency 4-6 ms) and polysynaptic activity (latency over 6-10 ms), both mediated by glutamate via AMPA receptors (Wallace, Jackson et al. 2014). There were no other components in field potentials, such as NMDA, kainate, or GABAergic transmission components, after CNQX and PTX block. VBs were removed entirely by blocking axonal transmission with 1 µM of Tetrodotoxin (TTX). Input-output curves are shown in Figure 6B as mean values of the first field potential amplitude. Pair-pulse facilitation was not different between the experimental groups (Figure 6B, one-way ANOVA $F_{5,18}= 0.75$, $p =0.57$), indicating that the glutamate release probability was not altered.

Synaptic excitability between the groups was compared using the amplitude of fEPSP at a stimulation intensity of 300 µA on input-output curves (Figure 6D, one-way ANOVA, $F_{5,18}= 11.42$, $p < 0.0001$) . Post-hoc multiple comparisons revealed that higher synaptic excitability in

sham IH animals (Fig. 6D) than Sham Normoxa (p<0.0001) was decreased after 1 Hz rTMS treatment (p=0.013) to the level not significantly different from Sham Normoxia.

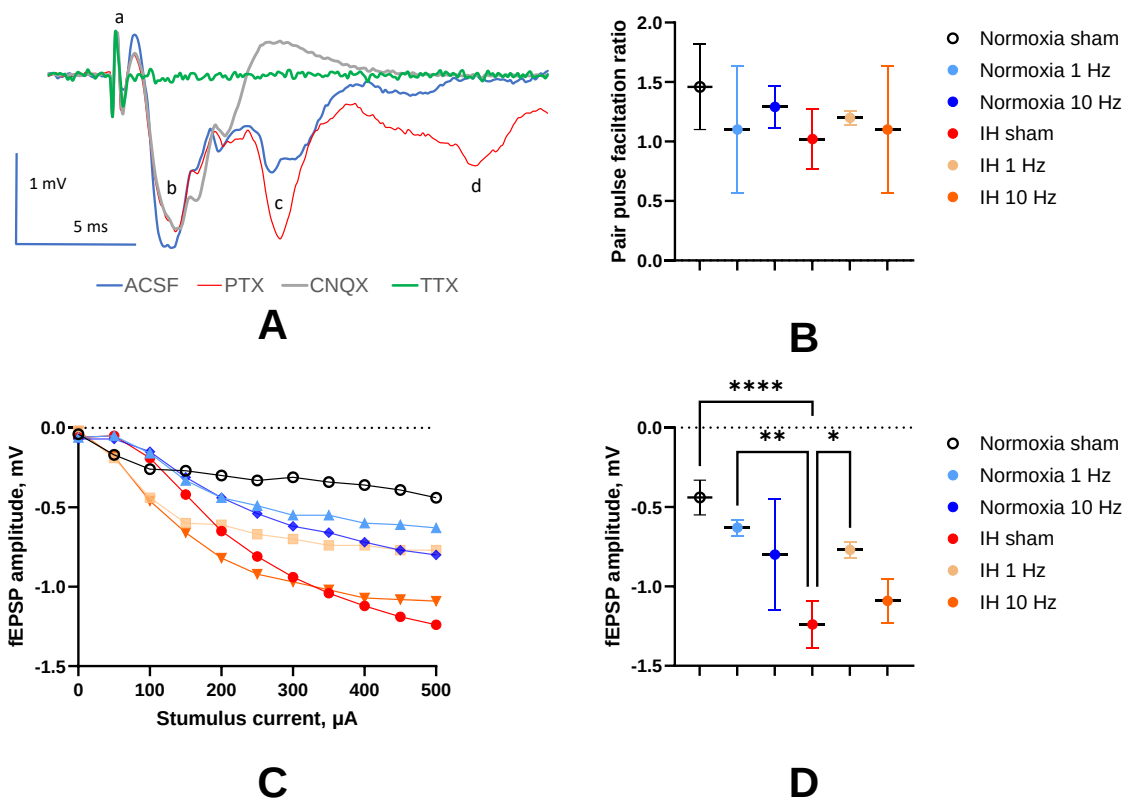

Figure 6 . Effect of IH and TMS on post-synaptic field potential in mouse motor cortex slices. A. Examples of fEPSP and waveforms originating at P70. a - truncated stimulation artefact, b – volley burst, c – first monosynaptic fEPSP, d- second polysynaptic fEPSP. The legend below shows inhibitors used to identify the origin of components. B. Pair pulse facilitation ratio was not different between the experimental groups. C. Input-out curves were quantified at stimulus intensity 500 µA with one-way ANOVA (D). Significance of post-hoc comparison is indicated as *- p<0.05, **-p<0.01, * p<0.001

DISCUSSION

This study employed a comprehensive approach, combining in vivo MRI, ex vivo electrophysiology, and behavioral assessments in a mouse model of neonatal IH to investigate the differential effects of LF- and HF-rTMS on cortical excitability and white matter myelination. This study found that HF-rTMS effectively ameliorated hypomyelination in the corticospinal tract. In contrast, LF-rTMS reduced locomotor hyperactivity and normalized elevated glutamatergic synaptic excitability after neonatal intermittent hypoxia. These differential effects highlight the potential of rTMS as a safe and targeted early intervention to address distinct neurological sequelae of perinatal hypoxic brain injury.

Safety and Anti-Inflammatory Aspects of rTMS

A critical prerequisite for any intervention in the vulnerable neonatal population is safety. Our results unequivocally demonstrate that the applied rTMS regimens, both low- and high-frequency, did not induce apoptosis or a generalized pro-inflammatory response in the neonatal mouse brain. This aligns with previous literature on the high safety margin of NIBS in pediatric settings (Gillick, Feyma et al. 2013, Gillick, Gordon et al. 2018). The observed decrease in TNF-α expression in the IH group after rTMS suggests a potential anti-inflammatory action, which could be a contributing mechanism to its therapeutic effects. Pro-inflammatory signals are known to influence oligodendrocyte lineage development negatively, potentially diverting them towards astrogenesis (Blaszczyk, Mohammadnia et al. 2025). Thus, the anti-inflammatory properties of rTMS, as suggested by our findings and prior stroke models (Buetefisch, Wei et al. 2023, Xing, Zhang et al. 2023, Peipei, Yu et al. 2024), and modulation of microglia by rTMS (d'Errico, Früholz et al. 2025) could play a crucial role in promoting myelin repair and recovery.

High-Frequency rTMS Ameliorates Hypomyelination.

A key finding of this study is the significant improvement in hypomyelination of the corticospinal tract following HF-rTMS after neonatal IH. As quantified by MPF maps, we observed a notable increase in myelin content in the internal capsule, both in the stimulated hemisphere and, notably, in the contralateral hemisphere. The profound and accelerated increase in MPF with HF-rTMS relative to sham in the IH group for the stimulated hemisphere highlights the potential of this stimulation paradigm to promote myelination, a critical process for efficient axonal conduction and functional motor control (Hunt, Neil et al. 2004). The bilateral effect, despite unilateral targeting, suggests a broader neuromodulatory influence of rTMS in the developing brain, potentially via interhemispheric connections or systemic effects. This finding addresses a critical gap identified in the introduction regarding the unexplored potential of non-invasive brain stimulation to promote myelination early after perinatal brain injury. While MPF changes were significant in the CST, no such effects were observed in the corpus callosum or cerebral cortex, indicating a degree of regional specificity or perhaps a need for different stimulation parameters to affect these areas. This regional specificity could be attributed to the nature of the perinatal injury model (primarily affecting CST) and the targeted stimulation, or it could suggest that myelination dynamics differ across brain regions and are differentially responsive to rTMS.

Low-Frequency rTMS Modulates Cortical Excitability and Behavior.

In contrast to the primary impact of HF-rTMS on myelination, low-frequency rTMS (LF-rTMS) demonstrated distinct therapeutic effects, specifically reducing locomotor hyperactivity and normalizing elevated glutamatergic synaptic excitability. Female IH mice exhibited significant hyperactivity in the open-field test, which was effectively reduced by LF-rTMS. This behavioral improvement was accompanied by a significant decrease in abnormally high glutamatergic synaptic excitability in motor cortex slices from IH animals treated with LF-rTMS. This normalization of synaptic function supports our hypothesis that LF-rTMS can counter the excessive glutamatergic transmission and subsequent occlusion of synaptic plasticity observed after neonatal IH (Goussakov, Synowiec et al. 2019, Goussakov, Synowiec et al. 2021). The anxiolytic effect of rTMS observed in both female and male mice further underscores its broader neurobehavioral benefits. This highlights LF-rTMS as a promising strategy to restore excitatory-inhibitory balance, a crucial aspect for normal brain development and function.

Differential Effects and Therapeutic Implications

The most striking implication of our findings is the clear differential effect of low- and high-frequency rTMS. HF-rTMS primarily enhanced myelination in the CST, crucial for motor control, while LF-rTMS targeted glutamatergic excitotoxicity and behavioral hyperactivity. This suggests that specific rTMS parameters may be tailored to address distinct pathological aspects of perinatal brain injury. Such precision could overcome limitations of pharmacological approaches, which often entail broad, long-term global inhibition with potentially disruptive consequences on the developing brain. The non-invasive nature and demonstrated safety profile of rTMS make it an attractive alternative for early intervention in a vulnerable population where timing and targeted therapies are critical for preventing the formation of pathological circuits and improving long-term outcomes.

Limitations and Future Directions

Despite these promising results, this study has several limitations. First, it was conducted in a mouse model, and caution must be exercised when translating findings directly to human infants. While mouse models provide valuable insights into underlying mechanisms, species-specific differences in brain development and responsiveness to rTMS exist. Second, our investigation into the molecular mechanisms underlying the observed effects is preliminary. Future studies should delve deeper into the cellular and molecular cascades triggered by different rTMS frequencies, particularly in terms of how they influence oligodendrocyte progenitor cell differentiation, maturation, and myelination, as well as the precise mechanisms of synaptic plasticity modulation. Investigations into inflammatory markers, such as specific pro- and anti-inflammatory cytokines, could further elucidate their role in rTMS-mediated amelioration of hypomyelination, as hypothesized.

Furthermore, while we observed positive effects on myelination and synaptic excitability, long-term follow-up studies extending beyond P70 are warranted to assess the persistence of these benefits and their impact on more complex cognitive and motor functions. Future research should also investigate the optimal timing, duration, and intensity of rTMS application, as well as the potential benefits of combining low- and high-frequency protocols, to maximize therapeutic efficacy. Ultimately, these preclinical findings lay a crucial foundation for future translational research and clinical trials investigating rTMS as an early, targeted intervention for improving neurodevelopmental outcomes in infants affected by perinatal hypoxic brain injury.

Conclusion.

Perinatal hypoxic brain injury is a significant clinical challenge, often resulting in complex neurodevelopmental disorders such as cerebral palsy and cognitive deficits. Current therapeutic strategies are largely palliative, underscoring the urgent need for effective early interventions that address the underlying pathophysiology. Our findings provide novel insights into the therapeutic potential of rTMS as a safe and effective neuromodulatory strategy for ameliorating key pathological hallmarks of perinatal hypoxic brain injury, including cortical hyperexcitability and white matter myelination deficits.

REFERENCES

Anderson, P. J. (2014). "Neuropsychological outcomes of children born very preterm." Semin Fetal Neonatal Med **19**(2): 90-96.

Babcock, M. A., F. V. Kostova, D. M. Ferriero, M. V. Johnston, J. E. Brunstrom, H. Hagberg and B. L. Maria (2009). "Injury to the Preterm Brain and Cerebral Palsy: Clinical Aspects, Molecular Mechanisms, Unanswered Questions, and Future Research Directions." Journal of Child Neurology **24**(9): 1064-1084.

Blaszczyk, G. J., A. Mohammadnia, V. E. C. Piscopo, J. Sirois, Q. L. Cui, M. Yaqubi, T. M. Durcan, R. Schneider and J. P. Antel (2025). "Pro-Inflammatory Molecules Implicated in Multiple Sclerosis Divert the Development of Human Oligodendrocyte Lineage Cells." Neurol Neuroimmunol Neuroinflamm **12**(4): e200407.

Boonzaier, J., P. I. Petrov, W. M. Otte, N. Smirnov, S. F. W. Neggers and R. M. Dijkhuizen (2020). "Design and Evaluation of a Rodent-Specific Transcranial Magnetic Stimulation Coil: An In Silico and In Vivo Validation Study." Neuromodulation **23**(3): 324-334.

Buetefisch, C. M., L. Wei, X. Gu, C. M. Epstein and S. P. Yu (2023). "Neuroprotection of Low-Frequency Repetitive Transcranial Magnetic Stimulation after Ischemic Stroke in Rats." Ann Neurol **93**(2): 336-347.

Burnett, A. C., S. E. Scratch and P. J. Anderson (2013). "Executive function outcome in preterm adolescents." Early Hum Dev **89**(4): 215-220.

Cahill-Rowley, K. and J. Rose (2014). "Etiology of impaired selective motor control: emerging evidence and its implications for research and treatment in cerebral palsy." Developmental Medicine & Child Neurology **56**(6): 522-528.

d'Errico, P., I. Früholz, M. Meyer-Luehmann and A. Vlachos (2025). "Neuroprotective and plasticity promoting effects of repetitive transcranial magnetic stimulation (rTMS): A role for microglia." Brain Stimulation: Basic, Translational, and Clinical Research in Neuromodulation **18**(3): 810-821.

Downing, A. L., K. J. Ganley, D. R. Fay and J. J. Abbas (2009). "Temporal characteristics of lower extremity moment generation in children with cerebral palsy." Muscle Nerve **39**(6): 800-809.

Gillick, B., T. Feyma, J. Menk and L. rach (2013). "Safety of transcranial direct current stimulation in pediatric hemiparesis: determining the optimal stimulation site." Developmental Medicine & Child Neurology **55**(Supplement s3).

Gillick, B. T., A. M. Gordon, T. Feyma, L. E. Krach, J. Carmel, T. L. Rich, Y. Bleyenheuft and K. Friel (2018). "Non-Invasive Brain Stimulation in Children With Unilateral Cerebral Palsy: A Protocol and Risk Mitigation Guide." Frontiers in Pediatrics **6**.

Goussakov, I., S. Synowiec, D. P. Aksenov and A. Drobyshevsky (2021). "Occlusion of activity dependent synaptic plasticity by late hypoxic long term potentiation after neonatal intermittent hypoxia." Exp Neurol **337**: 113575.

Goussakov, I., S. Synowiec, V. Yarnykh and A. Drobyshevsky (2019). "Immediate and delayed decrease of long term potentiation and memory deficits after neonatal intermittent hypoxia." Int J Dev Neurosci **74**: 27-37.

Hunt, R. W., J. J. Neil, L. T. Coleman, M. J. Kean and T. E. Inder (2004). "Apparent diffusion coefficient in the posterior limb of the internal capsule predicts outcome after perinatal asphyxia." Pediatrics **114**(4): 999-1003.

Hunt, R. W., J. J. Neil, L. T. Coleman, M. J. Kean and T. E. Inder (2004). "Apparent diffusion coefficient in the posterior limb of the internal capsule predicts outcome after perinatal asphyxia." Pediatrics **114**(4): 999-1003.

Johnson, S. and N. Marlow (2017). "Early and long-term outcome of infants born extremely preterm." Arch Dis Child **102**(1): 97-102.

Ketzer, C. R., C. Gallois, A. L. Martinez, L. A. Rohde and M. Schmitz (2012). "Is there an association between perinatal complications and attention-deficit/hyperactivity disorder-inattentive type in children and adolescents?" Revista Brasileira de Psiquiatria **34**(3): 321-328.
Krishnan, C., L. Santos, M. D. Peterson and M. Ehinger (2015). "Safety of noninvasive brain stimulation in children and adolescents." Brain Stimul **8**(1): 76-87.
Ma, D., M. J. Cardoso, M. Modat, N. Powell, J. Wells, H. Holmes, F. Wiseman, V. Tybulewicz, E. Fisher, M. F. Lythgoe and S. Ourselin (2014). "Automatic structural parcellation of mouse brain MRI using multi-atlas label fusion." PLoS One **9**(1): e86576.
Mikkelsen, S. H., J. Olsen, B. H. Bech, C. Wu, Z. Liew, M. Gissler, C. Obel and O. Arah (2017). "Birth asphyxia measured by the pH value of the umbilical cord blood may predict an increased risk of attention deficit hyperactivity disorder." Acta Paediatrica **106**(6): 944-952.
Milner-Brown, H. S. and R. D. Penn (1979). "Pathophysiological mechanisms in cerebral palsy." J Neurol Neurosurg Psychiatry **42**(7): 606-618.
Peipei, W., D. Yu, L. Xiaoyan, L. Yunxia, L. Liuming, C. Tongbin and L. Shaoping (2024). "Effects of a novel regimen of repetitive transcranial magnetic stimulation (rTMS) on neural remodeling and motor function in adult male mice with ischemic stroke." J Neurosci Res **102**(6): e25358.
Poon, D. M. and C. W. Hui-Chan (2009). "Hyperactive stretch reflexes, co-contraction, and muscle weakness in children with cerebral palsy." Dev Med Child Neurol **51**(2): 128-135.
Sukal-Moulton, T., K. J. Krosschell, D. J. Gaebler-Spira and J. P. Dewald (2014). "Motor impairment factors related to brain injury timing in early hemiparesis. Part I: expression of upper-extremity weakness." Neurorehabil Neural Repair **28**(1): 13-23.
Volpe, J. J. (2008). Neurology of the newborn. Philadelphia, Saunders/Elsevier.
Xing, Y., Y. Zhang, C. Li, L. Luo, Y. Hua, J. Hu and Y. Bai (2023). "Repetitive Transcranial Magnetic Stimulation of the Brain After Ischemic Stroke: Mechanisms from Animal Models." Cell Mol Neurobiol **43**(4): 1487-1497.
Yarnykh, V. L. (2007). "Actual flip-angle imaging in the pulsed steady state: a method for rapid three-dimensional mapping of the transmitted radiofrequency field." Magn Reson Med **57**(1): 192-200.
Yarnykh, V. L. (2016). "Time-efficient, high-resolution, whole brain three-dimensional macromolecular proton fraction mapping." Magn Reson Med **75**(5): 2100-2106.